Available online at www.eccomasproceedia.org
Eccomas Proceedia COMPDYN (2023) 4391-4401

ECCOMAS
Proceedia

COMPDYN 2023
9th ECCOMAS Thematic Conference on
Computational Methods in Structural Dynamics and Earthquake Engineering
M. Papadrakakis, M. Fragiadakis (eds.)
Athens, Greece, 12-14 June 2023

ML-BASED PUNCHING STRENGTH ESTIMATIONS OF FLAT SLABS WITHOUT TRANSVERSE REINFORCEMENT UNDER LATERAL LOADING

H. Panahi[1], **A. S. Genikomsou**[2]

[1] Ph.D. Candidate, Department of Civil Engineering, Queen's University, Kingston, ON, K7L 2N6, Canada
e-mail: Hadi.panahi@queensu.ca

[2] Assistant Professor, Department of Civil Engineering, Queen's University, Kingston, ON, K7L 2N6, Canada
ag176@queensu.ca

Abstract

Reinforced concrete flat plate systems are commonly used in North America due to their advantages such as the versatile architectural arrangements, ease of construction; however, these systems can be susceptible to brittle punching shear failure. As there is no other potential loading path after the occurrence of punching shear, this failure can lead to a progressive collapse of the structure. However, current design code provisions for punching shear are associated with high discrepancies for the punching shear strength estimation as they account for limited independent variables in their simple formulations and are mostly based on empirical equations derived from experimental data. Consequently, there is a need for proper numerical assessment of slab-column connections that can potentially lead to modifications to the design provisions. Due to the available uncertainties, a precise predictive tool is of great requirement. This study aims at applying machine-learning-based algorithms in the determination of punching shear capacity of slab-column connections without transverse reinforcement under both concentric vertical gravity forces and unbalanced moments due to lateral loadings. Herein, a Multilayer Perceptrons neural network model is trained using gradient descent and backpropagation algorithms. The performance of the developed model is further investigated by comparing its strength prediction with those of the available code provisions in which it is noted that the trained neural network showed higher accuracy.

Keywords: Flat Plate System, Machine Learning Technique, Unbalanced Moments, Drift, Code Provisions.

ISSN:2623-3347
Peer-review under responsibility of the organizing committee of COMPDYN 2023.
doi: 10.7712/120123.10727.20592

1 INTRODUCTION

The seismic performance-based design approach aims to accurately estimate the seismic functionality of structures and their advanced post-earthquake behavior for a wide range of earthquake scenarios. To achieve this, performance-based earthquake engineering requires the detection of various damage stages in structural elements, allowing for appropriate rehabilitation methods for existing structures or economically efficient design of new structures by predicting their hysteretic responses during earthquakes. One critical component in two-way flat plate systems is the reinforced concrete (RC) slab-column connection, as its integrity dictates the overall performance and global structural stability of the plate systems under lateral load demands. The governing brittle failure mode limiting the lateral deformation capacity of connections in flat plate systems is pure punching shear or flexural-punching failure, with potential for progressive collapse of the whole frame system. This study focuses on the behavior of slab-column connections under seismic loads using available experimental data and design provisions to determine their ultimate moment and drift capacities for seismic performance assessment.

Recent computational advancements have made machine learning (ML) techniques increasingly beneficial in structural and earthquake engineering. ML uses programming algorithms to optimize a performance index, based on available data. In structural engineering, researchers have applied ML models for strength regression, failure mode classification, damage assessment, and fragility curve regression (e.g., [1-7]). However, while these models can provide more accurate predictions than existing empirical formulations in flat plate systems, they are limited to slabs under monotonic vertical loading. A gap has also been identified in using ML methods to capture the limit states of RC slab-column connections subjected to unbalanced moments. Additionally, due to the lack of an adequate dataset on slabs under lateral loading, ML models are crucial in accurately predicting the drift capacity of slabs. Therefore, ML algorithms are used to fit models for estimating the ultimate moment strength and drift capacity of slab-column connections at the failure point under lateral cyclic loading.

Currently, non-linear parameters available in ASCE 41-17 [8], empirically defined equations such as the bilinear equation in ACI 318-19 [9], the hyperbolic equation in CSA A23.3-19 [10], or the double bilinear equations proposed by Zhou and Hueste [11], and mechanical models proposed by Drakatos et al. [12], Setiawan et al. [13], Broms [14], and Muttoni et al. [15], can be used to determine the drift-based backbone response as the limit state of slab-column connections for numerical analysis. However, empirically defined equations have limited independent variables and provide lower or average bounds for the design drift. Furthermore, code provisions are mostly based on limited experimental data obtained from small-scale isolated interior slab-column connections, making them less reliable for numerical analysis. Therefore, the derivation of a precise regression that can be employed for failure recognition in numerical analysis/design requires intricate solutions.

Predicting the unbalanced moment resistance and contribution of each lateral-load resisting mechanism (i.e., flexure, torsion, and eccentric shear) to the overall strength of slab-column connections is complex due to their non-linear behavior. In ACI 318-19 [9] design code, a fraction of column side lengths is adopted to relate the contribution of shear (γ_v) and flexural (γ_f) mechanisms, and the torsion mechanism is neglected. While the column is square, the eccentric shear and flexure mechanism coefficients are 0.4 and 0.6, respectively. ACI 318-19 [9] recommends a formula for unbalanced moment resistance, which is a function of initial vertical loading, the fraction of resisting mechanism coefficients, the polar moment of inertia, and the punching shear strength of the connection. The unbalanced moment resistance determined by EC2-2004 [16] includes different mechanism contribution coefficients, punching shear

strength with various variables, and a different polar moment of inertia. CSA A23.3-19 [10] provides an equation for unbalanced moment prediction of slabs similar to ACI 318-19 [9]; however, the punching shear capacity of concrete is with different coefficients. The available design codes include several shortcomings. The contribution of eccentric shear force and flexure mechanisms considered in all design provisions are constant for any drift limits; however, the actual behavior of the slab connections subjected to lateral loading represents variable mechanism coefficients. Moreover, the design provisions are based on experimental and empirical research while neglecting the contribution of the torsion mechanism. Furthermore, the existing design practices assume a linear distribution of shear stresses on the critical perimeter while it is non-linear in reality.

Therefore, this paper aims to propose more accurate formulations for estimating the unbalanced moment and drift capacities of slabs under lateral loading, taking into account the variable nature of the flat slab design procedure, performance requirements, and various geometric and material properties. To achieve this, 105 interior moment-resisting slab-column specimens without shear reinforcement under (monotonic or cyclic) lateral loading are analyzed using different ML models, including decision trees, random forests, support vector machines (SVMs), and deep neural network (NN) algorithms. The proposed models correlate slab moment and drift capacities with ten independent parameters, including slab side lengths (l_1 and l_2), column side lengths (c_1 and c_2), slab thickness (h), average effective depth (d), flexural reinforcement ratio (ρ), compressive strength of concrete (f_c'), the initial vertical gravity load (V_g), and the lateral loading type (LT). Results show that the deep NN model is the most suitable for estimating drift limit and moment capacity.

2 DATA COLLECTION

The present study compiled a database of 105 RC two-way flat slab specimens subjected to lateral loading, sourced from various research articles and dissertations. These specimens included small-scale or full-scale experiments and frame assemblies of interior slabs or interior continuous connections without transverse reinforcement under gravity and lateral (monotonic or uniaxial/biaxial cyclic) loadings. Pearson's method was used to estimate the standard correlation coefficient of the dataset, as shown in Figure 1, which demonstrates the strong correlation between the moment and drift values at the failure of the slab-column connection and the slab and column geometry, material properties, and loading parameters. The input features considered in this study comprise a 10-dimensional vector, including slab dimensions, slab thickness, average effective depth, column sides, concrete compressive strength, flexural reinforcement ratio, initial vertical gravity load, and lateral loading type. Table 1 shows the mean and standard deviation of each model feature, while Figure 2 displays the distributions of the key parameters selected to characterize the drift and moment capacities of the two-way flat slabs.

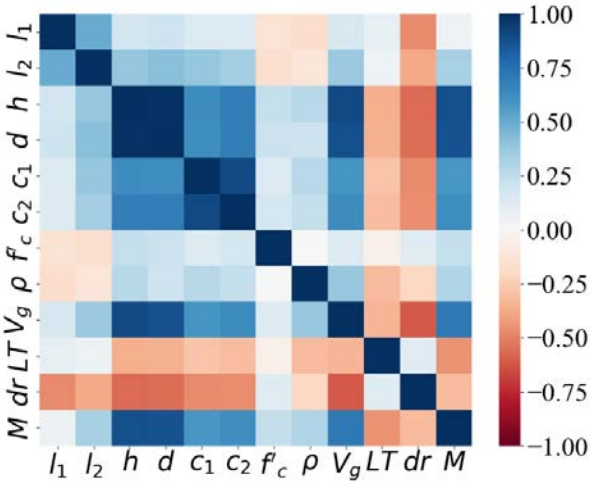

Figure 1. Correlation heat map between the features.

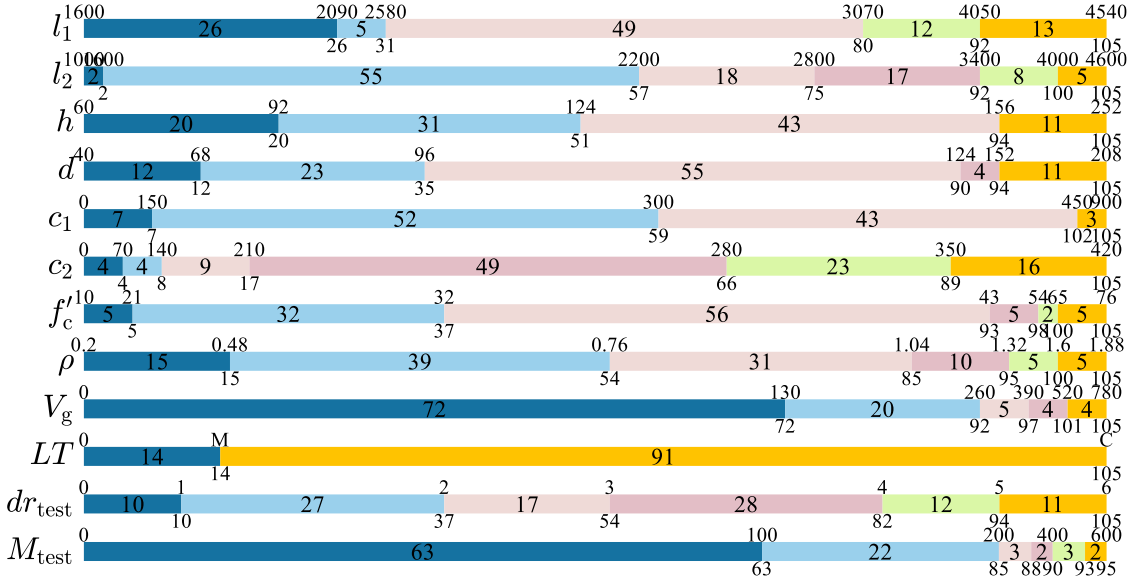

Figure 2. Distribution of features. The number inside the bars shows the number of specimens in each range, the top number shows the value of each range for the relevant feature, and the bottom number indicates the accumulated number of specimens until that value.

Table 1. Mean and standard deviation of model features.

Feature/Output	Notation	Mean/Count	Standard Deviation
Slab length parallel to loading dir. (mm)	l_1	2910	804
Slab length normal to loading dir. (mm)	l_2	2433	733
Slab thickness (mm)	h	137	47
Average effective depth (mm)	d	109	37
Column side parallel to loading dir. (mm)	c_1	290	130
Column side normal to loading dir. (mm)	c_2	265	80
Concrete compressive strength (MPa)	f'_c	34.98	11.21
Flexural reinforcement ratio (%)	ρ	0.794	0.345
Initial vertical gravity load (kN)	V_g	143.96	160.23
Lateral loading type: monotonic/cyclic	LT	91/14	-
Drift ratio at punching failure (%)	dr	2.77	1.45
Moment at punching failure (kN.m)	M	106.14	113.27

3 PREDICTIONS BY AVAILABLE EQUATIONS

3.1 Drift Prediction

The scatter plot in Figure 3 shows the relationship between the drift limit state of the collected database and GSR, along with the predicted drift values by the empirical equations provided by ACI 318-19 [9], ASCE 41-17 [8], CSA A23.3-19 [10], and Zhou and Hueste [11]. Drakatos et al. [12] and Muttoni et al. [15] are excluded from the figure as their mechanical models do not have a specific shape concerning GSR values. The empirically defined equations have limited independent variables and give lower or average bounds for the design drift. Figure 3 also shows that while the increase of initial gravity load leads to a degradation of the lateral load resisting capacity of the connections and vice versa, the experimental test data of interior slab-column connections without transverse reinforcement subjected to lateral monotonic or seismic actions demonstrate that the deformation capacity of the connections is not perfectly correlated with GSR. As a result, it is not possible to accurately estimate the drift capacity of slabs with a simple equation and requires a point-prediction method such as ML algorithms.

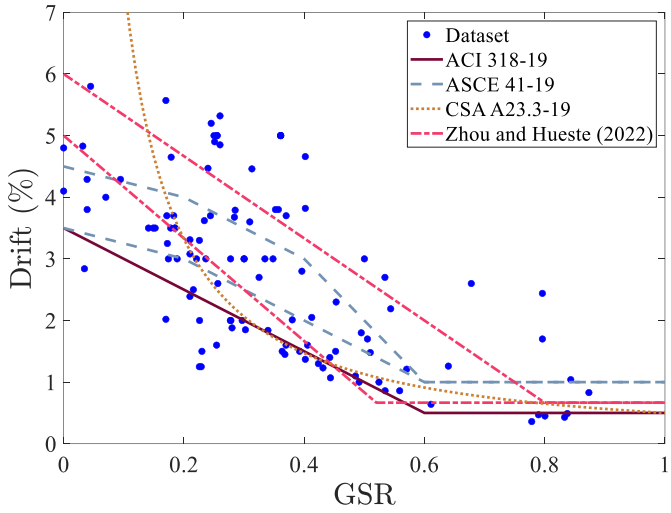

Figure 3. Accumulated dataset and its comparison to the design codes and empirical predictions.

Figure 4 compares the design code provisions with available empirical and mechanical equations in terms of predicted and experimental drift capacity values. The accuracy indices such as coefficient of determination, R^2, mean absolute error, MAE, the root of mean square error, $RMSE$, and the coefficient of variation values, COV are used for comparison. The R^2 for ACI 318-9 and CSA A.23.3-19 [9, 10] are negative values, and for estimations by Muttoni et al., Zhou and Heuste, and ASCE 41-17 [8, 11, 15] are 2%, 43%, and 45%, respectively. The shortcoming of available empirical models in identifying accurate lateral drift limit of slab-column connections is conspicuous. As the mechanical model of Drakatos et al. [12] requires maximum aggregate size and the yield stress capacity of tensile flexural reinforcements, which are not available for 72 specimens of the dataset, these data are excluded, as shown in Figure 4-f, and the accuracy indices are among just 33 specimens. As shown in Figure 4-a, b, and d, since ACI 318-19, ASCE 41-17, and Zhou and Hueste [8, 9, 11] restrain the drift values as a lower bound at 0.5, 1.0, and 0.67%, respectively, the predicted drift capacities could not go lower than these values. Conversely, there are five slabs that failed at drift lower than 0.5% and 11 slabs at lower than 1.0%.

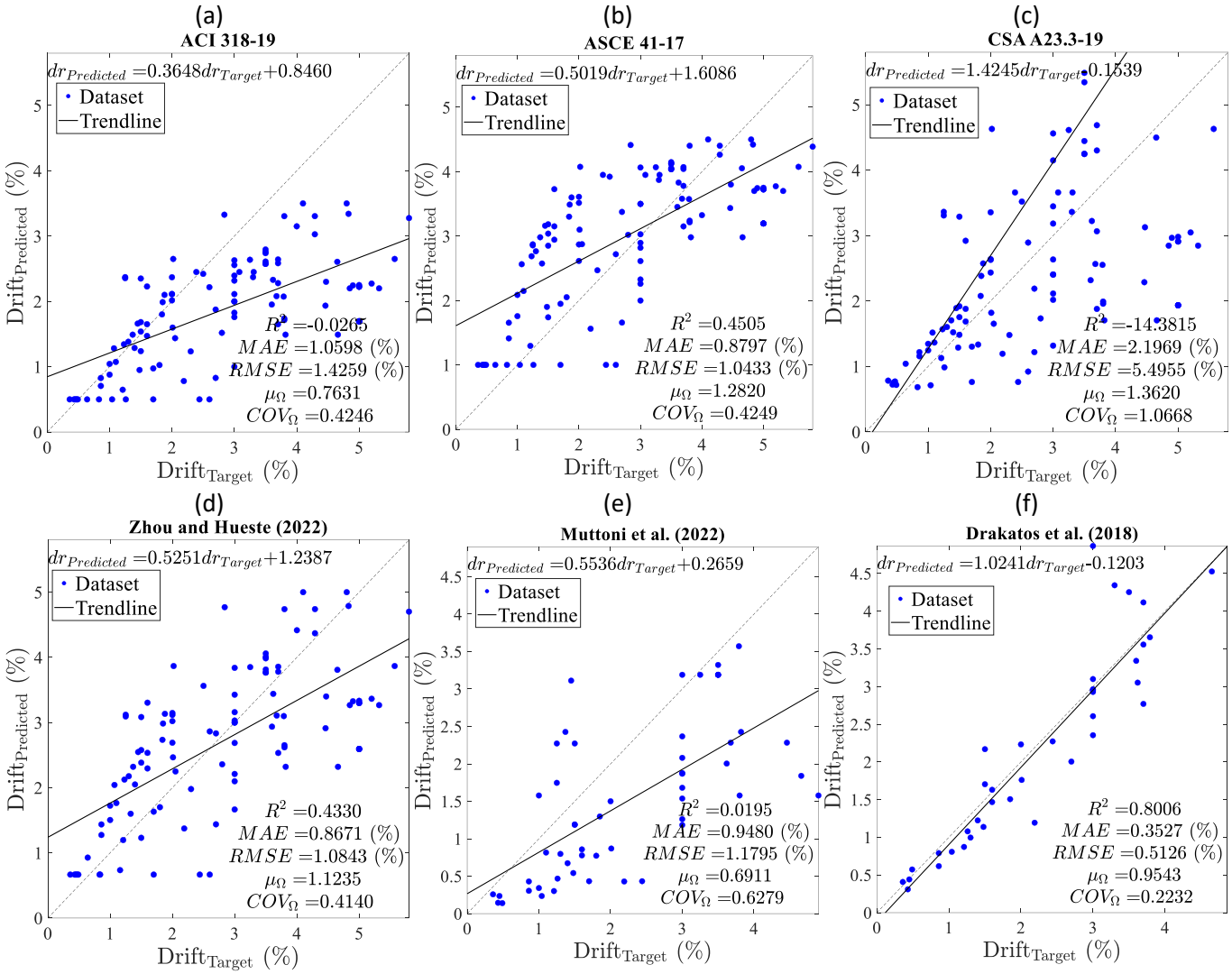

Figure 4. Comparison of the prediction model results versus actual experimental data for drift at punching failure: a) ACI 318-19 [9], b) ASCE 41-17 [8], c) CSA A.23.3-19 [10], d) Zhou and Hueste [11], e) Muttoni et al. [15], and f) Drakatos et al. [12].

3.2 Unbalanced Moment Prediction

Figure 5 compares the prediction and experimental target values for unbalanced moments of the collected data among different design codes. It is observed that EC2-2004 [16] performs better in terms of R^2, MAE and $RMSE$ indices for the capacity of connections regarding the unbalanced moment, followed by CSA A23.3-19 and ACI 318-19, respectively. This difference may be attributed to the inclusion of the flexural reinforcement effect in EC2-2004's punching shear strength equation, which is not considered in ACI 318-19 and CSA A23.3-19.

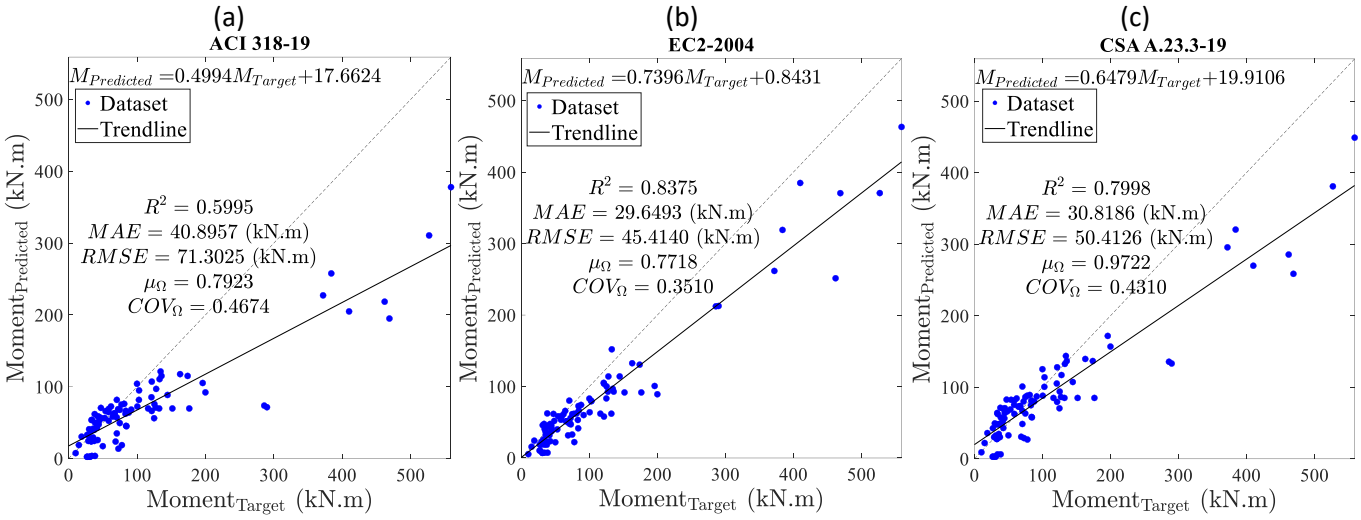

Figure 5. Comparison of the prediction model results versus actual experimental data for the unbalanced moment at punching failure: a) ACI 318-19 [9], b) EC2-2004 [16], and c) CSA A.23.3-19 [10].

4 MACHINE LEARNING METHODS

In this section, various ML algorithms are used to assess their performance regarding drift and unbalanced moment strengths prediction of the collected data.

4.1 Decision Trees

Decision trees are versatile ML algorithms that can perform regression fitting of complex datasets. These are fundamental components of the random forests model, which are among the most powerful ML models available today. One of the qualities of decision trees is that they do not require special preprocessing and feature scaling. The CART optimization algorithm is adopted to train growing trees. This greedy algorithm works by first splitting the training dataset in a way to minimize the MSE. This model is often called a non-parametric model, not because it does not require any parameters but because the number of parameters is not determined prior to the training. Thereby, the structure of the model is free to stick to the data, and they are prone to overfitting. Hence, it is needed to set some hyperparameters, such as the minimum number of samples of a leaf node that is set to 2 and the maximum depth of the tree, which is tuned to five.

4.2 Random Forests

The random forests algorithm is mainly an ensemble of many decision trees on a random subset of features in which each tree is grown by a random bootstrap sample of a training dataset and then averaged out their prediction. At each node of the tree, a randomly chosen subset of features is used to generate the best partitioning. The training procedure continues until each point in the sample is assigned to a terminal node from previously partitioned nodes and is repeated until the desired number of trees has been grown. The trained model includes 100 trees in the forest with the maximum depth of the tree equal to five. The minimum number of samples required to be at a leaf node is set to 2 in order to overcome overfitting.

4.3 Support Vector Machines

SVMs for regression (known as support vector regression, SVR) is a kind of ML algorithm capable of linear and non-linear regression for small to medium-sized datasets. SVR tries to

fit as many samples as possible on the street while limiting margin violations. Since it is prone to overfitting L2 regularization is adopted. The non-linear SVR model is trained with the RBF kernel with degree of the polynomial kernel function equal to 10.

4.4 Deep Neural Network

NNs are versatile, powerful, and ideal to tackle large and highly complex ML tasks. Thereby, a deep NN, which is heavily used today, is established to fit a non-linear regression for the deformation capacity of RC two-way flat slabs without transverse reinforcement. NN models are comprised of weights and biases (i.e., unknown model parameters) in which these values have been calculated so that the model best fits the training set by optimizing a cost function. In this study, a deep NN module is developed using the Nadam optimization algorithm in a deep network, as Nadam optimization outperforms in this regard. The hyperparameters of the model, including the number of hidden layers, the number of neurons in each layer, the learning rate, and activation functions, are tuned after multiple trials and errors. The developed NN architecture, as shown in Figure 6, includes ten neurons in the input layer, 128, 256, 256, 256, 128, and 64 neurons in six hidden layers, and a neuron in the output layer as the estimated value for the lateral drift or unbalanced moment capacity of slabs. The value of each neuron in hidden and output layers is determined by the activation of neurons in the previous layer using the activation function. Herein, the *ReLU function* is adopted as an activation function for neurons. Since the range of input features is different, it is needed to standardize all the input and output features of the dataset by Equation (1).

$$x_j = (x - x_{\min})/(x_{\max} - x_{\min}) \tag{1}$$

Where, $x_{\max}$ and $x_{\min}$ are the maximum and minimum values among all values of feature x in the training set or test set.

Mean squared error (MSE) formulation, as expressed in Equation (2), is adopted as a cost function, C, of the network to evaluate the accuracy of the model in each iteration (epoch).

$$C(w,b) = \mathrm{MSE}(y,a) = \frac{1}{n}\sum_{j=1}^{n}\left\|y_j(x) - a_j\right\|^2 \tag{2}$$

Here, w denotes the collection of all weights in the network, b presents all the biases, n is the total number of training inputs, y is the desired target drift capacity (from test data), a is the vector of outputs from the network when x_j is input, and the sum is over all training inputs, x. The training of weights and biases of the artificial network is carried out using the Nadam algorithm in Python. The training procedure is monitored after each epoch to avoid underfitting the model, and the L2 regularization penalty is applied to the model to avoid overfitting.

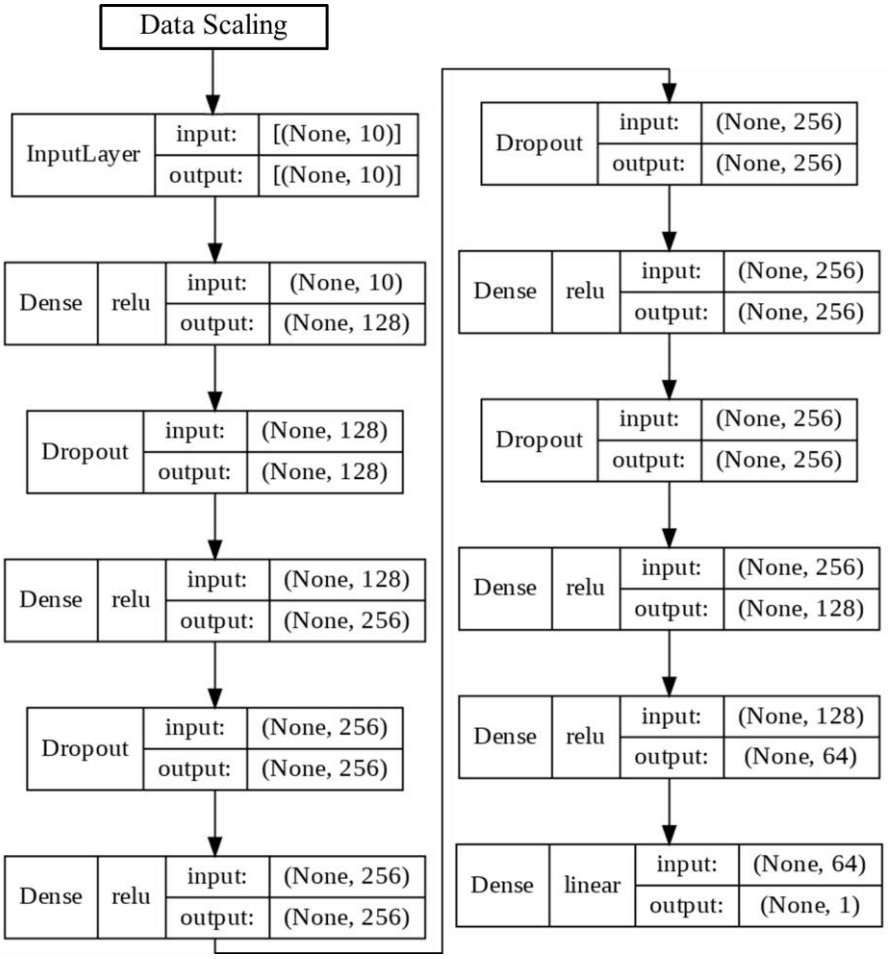

Figure 6. Assumed architecture for the deep NN model.

4.5 Training of the Accumulated Dataset

To assess which ML method is suited for the training of data, a preliminary analysis is conducted in which linear regression, decision tree, linear SVR, SVR, and random forests algorithms, as well as a deep neural network, were tested using Tensorflow and Scikit-learn modules available in Python programming language and by applying a k-fold cross validation of 12 splits. The dataset is split into 70% as a training set (for fitting the model) and 30% as a test set (to evaluate the trained model) that are randomly sampled. Table 2 lists the models tested along with their performance measures. Based on Table 2, the deep neural network model achieved the highest performance in R^2, MAE, and mean square error, MSE, values followed by the decision trees and random forests models, respectively, while the remaining models showed less suitable performance regarding predicting drift or moment estimation.

The fitted data along with the actual experimental drift and moment values are compared in Figure 7-a and -b, respectively, for the deep NN model. According to Figure 7, Figure 4, and Figure 5, the trained deep NN estimated the drift capacity of the connections with 41% and 42% higher accuracy than ASCE 41-17 [8] and Zhou and Hueste's model [11], respectively, and the unbalanced moment capacity with 31% and 22% higher precision than CSA A23.3-19 and EC2-2004.

Table 2. ML regression models results.

ML Regression Model	*Total Data*					
	Drift			*Moment*		
	R^2	*MAE*	*MSE*	R^2	*MAE*	*MSE*
Linear regression	0.530	0.81	0.97	0.642	29.18	602.10
Decision trees	0.854	0.36	0.30	0.884	27.78	502.90
Linear SVR	0.356	0.90	1.34	0.501	33.20	607.89
SVR	0.799	0.30	0.42	0.834	21.95	502.42
Random forests	0.840	0.43	0.33	0.878	34.10	510.67
Deep neural network	0.856	0.38	0.30	0.961	22.40	501.58

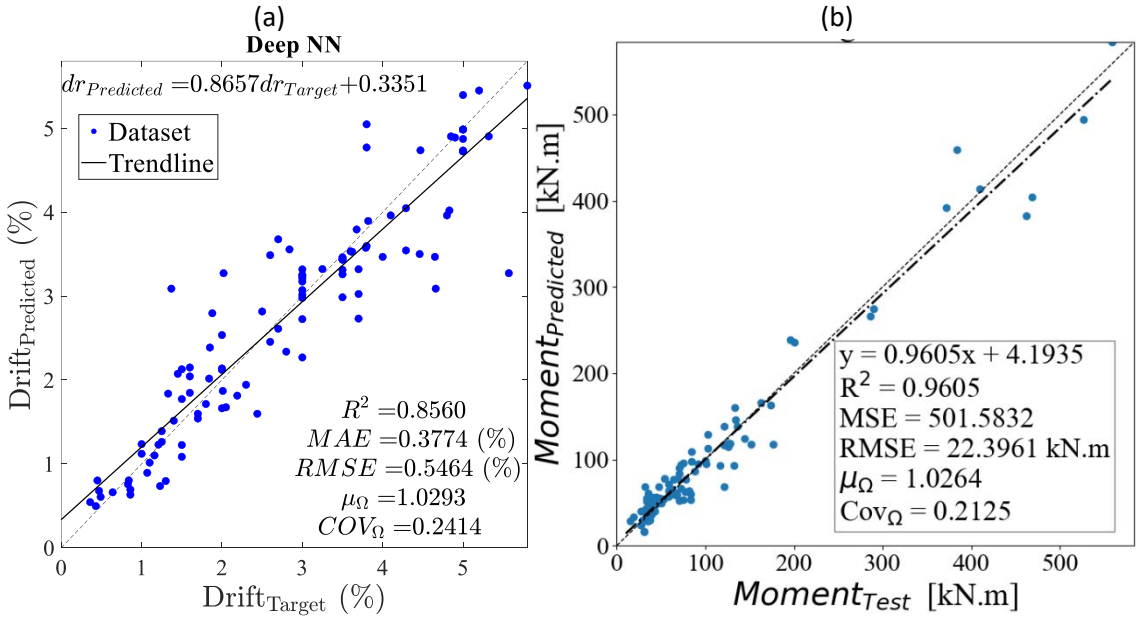

Figure 7. Comparison of the accumulated experimental data with predicted values by the developed deep NN model for a) drift at the punching failure and b) moment at the punching failure.

5 CONCLUSIONS

Based on the collected data and the machine learning analysis results, the following conclusions can be drawn:

- Available design code equations are conservative for assessing the seismic performance of these connections regarding unbalanced moment or drift capacities.
- The various empirical models to estimate the drift limit states of the connections are not precise for the seismic assessment of buildings with flat plate systems.
- A dataset of 105 experimental test results of small-scale and full-scale, as well as frame assemblies of interior slabs without transverse reinforcement under both gravity and lateral (monotonic or uniaxial/biaxial cyclic) loadings was collected.
- Various machine learning algorithms are trained, and the deep neural network model outperformed in predicting slab drift limit states and moment strengths under lateral loading.

REFERENCES

1. Chetchotisak, P., et al., *Punching shear strengths of RC slab-column connections: Prediction and reliability.* KSCE Journal of Civil Engineering, 2018. **22**(8): p. 3066-3076.
2. Mangalathu, S. and J.-S. Jeon, *Classification of failure mode and prediction of shear strength for reinforced concrete beam-column joints using machine learning techniques.* Engineering Structures, 2018. **160**: p. 85-94.
3. Abambres, M. and E.O. Lantsoght, *Neural network-based formula for shear capacity prediction of one-way slabs under concentrated loads.* Engineering Structures, 2020. **211**: p. 110501.
4. Chen, P.-Y., Z.Y. Wu, and E. Taciroglu, *Classification of Soft-Story Buildings Using Deep Learning with Density Features Extracted from 3D Point Clouds.* Journal of Computing in Civil Engineering, 2021. **35**(3): p. 04021005.
5. Tran, V.-L. and S.-E. Kim, *A practical ANN model for predicting the PSS of two-way reinforced concrete slabs.* Engineering with Computers, 2021. **37**(3): p. 2303-2327.
6. Mangalathu, S., et al., *Explainable machine learning models for punching shear strength estimation of flat slabs without transverse reinforcement.* Journal of Building Engineering, 2021. **39**: p. 102300.
7. Asteris, P.G., et al., *Predicting the shear strength of reinforced concrete beams using Artificial Neural Networks.* Computers and Concrete, An International Journal, 2019. **24**(5): p. 469-488.
8. ASCE/SEI. *Seismic evaluation and retrofit of existing buildings*. 2017. American Society of Civil Engineers.
9. ACI. *ACI CODE-318-19: Building Code Requirements for Structural Concrete and Commentary*. 2019. American Concrete Institute.
10. CSA. *CSA A23.3-19: Design of Concrete Structures*. 2019. Canadian Standards Association.
11. Zhou, Y. and M.B.D. Hueste, *Nonlinear Modeling Parameters and Acceptance Criteria for Interior Slab-Column Connections.* ACI Structural Journal, 2022. **119**(1): p. 145-154.
12. Drakatos, I.-S., A. Muttoni, and K. Beyer, *Mechanical model for drift-induced punching of slab-column connections without transverse reinforcement.* ACI Structural Journal, 2018. **115**(2): p. 463-474.
13. Setiawan, A., R.L. Vollum, and L. Macorini, *Numerical and analytical investigation of internal slab-column connections subject to cyclic loading.* Engineering Structures, 2019. **184**: p. 535-554.
14. Broms, C., *Structural Model for Interstory Drift Capacity of Flat Slabs without Shear Reinforcement.* ACI Structural Journal, 2020. **117**(3).
15. Muttoni, A., et al., *Deformation capacity evaluation for flat slab seismic design.* Bulletin of Earthquake Engineering, 2022: p. 1-36.
16. Européen, C., *Eurocode 2: Design of concrete structures—Part 1-1: General rules and rules for buildings.* London: British Standard Institution, 2004.